Geochemical Perspectives Letters

Ion imaging of ancient zircon

C.L. Kirkland[1†*], T.E. Johnson[1], J. Gillespie[1,‡], L. Martin[2]

https://doi.org/10.7185/geochemlet.2332

Abstract

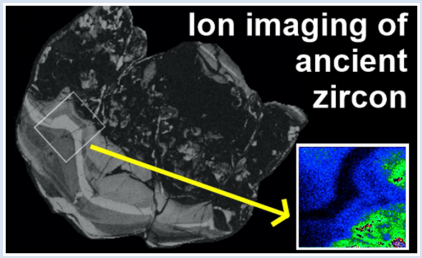

The Idiwhaa gneiss, part of the Acasta Gneiss Complex, Canada, is a key source of information concerning formation of continental crust on the early Earth. However, zircon crystals from this oldest dated felsic crust were affected by multiple stages of alteration and metamorphism, leading to difficulties in disentangling primary from secondary processes. These grains provide an opportunity to understand the alteration processes that affect ancient zircon crystals. Ion imaging reveals pervasive recrystallisation fronts extending inwards from the margins of grains. Ahead of these recrystallisation fronts, grain cores contain isolated pockets of amorphous, but concordant, 3.99 Ga zircon that evidently escaped post-magmatic modification of U and Pb. The transport of these elements, involving the decoupling of parent and daughter isotopes, is highly heterogeneous over space and time within metamict zircon, yet localised domains still retain primary age information. Our data indicate that metamictisation of zircon alone does not lead to radiogenic Pb loss, which requires interaction with fluid.

Received 30 June 2023 | Accepted 31 August 2023 | Published 5 October 2023

Introduction

The rarity of unaltered igneous rocks that formed earlier than three billion years ago (>3 Ga) leads to considerable uncertainty in tracking the development of nascent continental crust and in understanding the establishment of, and recycling between, long-lived geochemical reservoirs that ultimately maintained life (Ward and Brownlee, 2000; Willbold *et al.*, 2015). In our quest to better understand the early Earth (Hadean to Eoarchean; ≥3.6 Ga), analysis of the date, trace element, and isotopic composition of zircon crystals has been fundamental (Harley and Kelly, 2007; Valley *et al.*, 2015; Trail *et al.*, 2016). Although U–Pb isotopic ratios in ancient zircon grains are potentially easier to measure due to protracted radiogenic Pb ingrowth, such grains frequently show evidence for radiation damage that variably may disturb their primary crystal chemical and isotopic compositions (Pidgeon *et al.*, 2017). Radiation damage generates pathways for fluids whose passage through the crystal may modify the composition of zircon by removing Pb and/or facilitating uptake of other non-formula elements (Nasdala, 1998). However, the effects of radiogenic Pb loss can be difficult to disentangle from other secondary processes, including recrystallisation, diffusion, and growth of new zircon, all of which may occur in response to tectonothermal disturbance and/or fluid ingress. The effects of these secondary processes can alter the primary chemical composition of zircon and are mostly cumulative such that their effects increase with age.

The Acasta Gneiss Complex (AGC) in Northwest Territories, Canada (Supplementary Fig. S-1), contains the oldest known evolved rocks on Earth, the tonalitic Idiwhaa gneiss, which contains zircon grains preserving U–Pb crystallisation ages as old as *ca.* 4.03 Ga (Stern and Bleeker, 1998; Bowring and Williams, 1999; Reimink *et al.*, 2014, 2016). However, the rocks preserve evidence for a complex Pb-loss history such that the primary processes involved in their formation are difficult to disentangle (Moorbath *et al.*, 1997; Reimink *et al.*, 2014, 2016; Kirkland *et al.*, 2020). Here, we investigate a sample (AC13) of the Idiwhaa gneiss using a multi-technique approach combining optical, secondary electron, electron-backscattered diffraction (EBSD), cathodoluminescence (CL) imaging, and secondary ionisation mass spectrometry spot analyses of zircon grains with detailed ion imaging (mapping) of selected grains. Previous ion imaging studies of ancient zircon elsewhere have implied variable intra-crystalline radiogenic Pb mobility (Kusiak *et al.*, 2013; Ge *et al.*, 2018, 2019). Data from the Idiwhaa gneiss provide insight into the processes of zircon growth and modification of Earth's oldest known continental crust.

Sample and Method

Sample AC13 contains mainly quartz and plagioclase, with less biotite, hornblende, and garnet, and accessory magnetite, ilmenite, apatite, and zircon. The rock is a banded gneiss with felsic (quartzofeldspathic) and more mafic layers, the latter dominated by hornblende, with minor garnet, and biotite, that define a foliation. The matrix comprises subequal proportions of quartz and plagioclase interspersed with finer-grained biotite. Limited greenschist-facies alteration is evident through sericitisation of plagioclase and partial chloritisation of biotite along cleavage planes (Supplementary Fig. S-2).

1. (†Timescales of Mineral Systems Group), School of Earth and Planetary Sciences, Curtin University, Perth, WA 6845, Australia
2. Centre for Microscopy Characterisation and Analysis, The University of Western Australia, Perth, WA 6009, Australia
‡ Current address: Institute of Earth Sciences, Faculty of Geosciences and Environment, University of Lausanne, Lausanne CH-1015, Switzerland
* Corresponding author (e-mail: C.Kirkland@curtin.edu.au)

Zircon crystals from sample AC13 were analysed for U–Pb isotopes using the SHRIMP II ion probe at Curtin University. Following SHRIMP analysis, ion imaging of zircon was performed on a Cameca 1280 ion microprobe at the University of Western Australia. The detailed analytical procedures are described in the Supplemental Information. The U–Pb data table and apparent dates based on ion mapping are given in Supplementary Data Tables S-1 and S-2, respectively. All uncertainties within the text are quoted at the 2σ level.

Zircon U–Pb Date and Internal Textures

Zircon grains from sample AC13 are subhedral, have moderate length-to-width ratios and are brown under transmitted light. Based on cathodoluminescence (CL) images, their internal features can be simplified into three distinctive textural components (CL types 1–3) (Fig. 1). Highly-metamict cores (CL type 1) generally show low response and mottled CL emissions, contain abundant inclusions, and are commonly traversed by high CL response fractures. Electron backscattered diffraction (EBSD) analysis reveals the cores to be largely composed of low-crystallinity zircon, with patchy areas of more crystalline zircon within the mottled CL texture domains. The cores are bordered by discontinuous zones (CL type 2) up to 30 μm thick that parallel feint ('ghost') oscillatory zoning interpreted to reflect primary magmatic growth (Geisler *et al.*, 2007; Harley *et al.*, 2007). Analysis by EBSD shows that CL type 2 zircon is highly crystalline, typically comprising a low CL response inner band with indistinct, broad zoning that transitions to an outer band with a discrete high CL response. The internal texture of CL type 2 reveals inward-facing cuspate textures at sites where fractures are now centred (Fig. 1). Domains of CL type 2 are surrounded by more homogeneous low CL response rims (CL type 3) that form the outermost edge of the grains. The inner edge of CL type 2 has a convoluted margin against CL type 1, but a more regular contact against CL type 3 rims (Fig. 1).

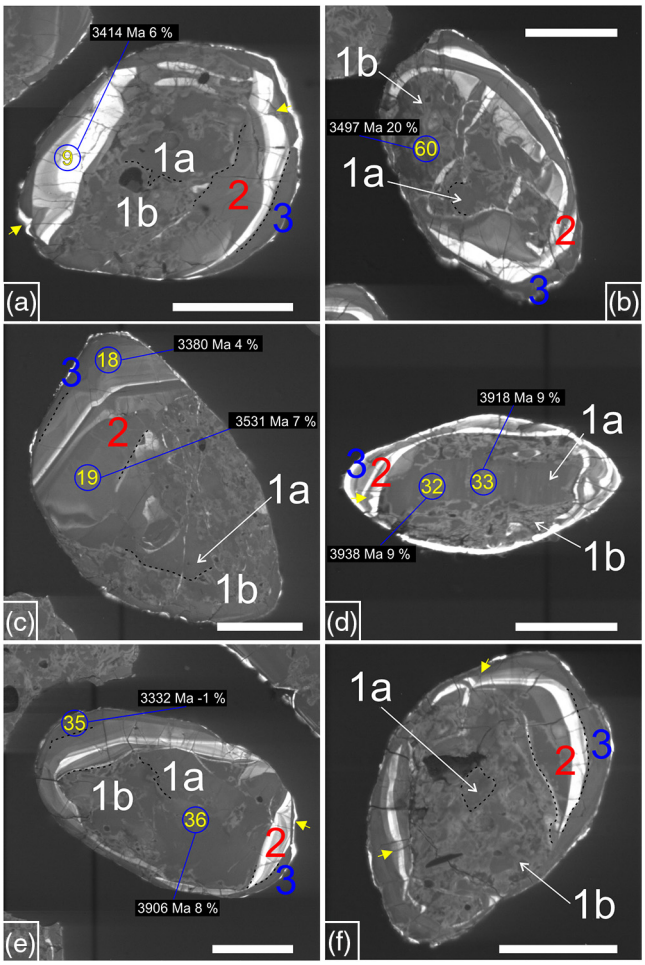

Figure 1 (a–f) Representative CL images of AC13 zircon. U–Pb spots are blue ellipses. Numbers indicate the CL types 1–3 (white, red, and blue font). Yellow arrows indicate cuspate zonation centred on fractures. $^{207}Pb^*/^{206}Pb^*$ dates and discordance % in white font. Scale bars are 100 μm.

Eighty-six U–Pb SIMS spot analyses were obtained from 44 zircon grains. Results are listed in Supplementary Data Table S-1 and illustrated in Figure 2. The analyses are concordant to strongly discordant and scatter away from several apparently concordant Hadean to Archean components. Sixty-five analyses targeting a range of internal textures within the CL type 1 cores, characterised by mottled and patchy CL zonation, are >5 % discordant (Group D). The most discordant of these analyses are sited within inclusion-rich metamict zircon. Based on internal textures and U–Pb systematics, zircon grains within 5 % of concordia can be grouped into at least three components. Group 1a comprises three analyses on the core of a single grain with homogenous CL type 1 textures and low crystallinity (Supplementary Data Table S-1), data from which yield a weighted mean $^{207}Pb^*/^{206}Pb^*$ date of 3990 ± 2 Ma (MSWD = 0.4). Ten analyses on more heterogeneously-textured CL type 1 core domains (Group 1b) have $^{207}Pb^*/^{206}Pb^*$ dates ranging from 3973–3780 Ma. Group 2 comprises four analyses targeting CL type 2 transgressive veins and fronts that yield $^{207}Pb^*/^{206}Pb^*$ dates of 3520–3380 Ma. A single analysis (Group 3) on a homogeneous CL type 3 rim yields a $^{207}Pb^*/^{206}Pb^*$ date of 3332 ± 12 Ma.

Ion and EBSD imaging of two zircon grains that preserve the various CL textures discussed above was undertaken (Supplementary Fig. S-3). Grain X comprises an amorphous core with $^{207}Pb^*/^{206}Pb^*$ date of 3990 Ma (Group 1a) and is transgressed by high-CL response, low-U veins associated with $^{207}Pb^*/^{206}Pb^*$ dates of 3973–3780 Ma (Group 1b). The edge domain of this grain (CL type 2) has a more homogeneous CL response and higher EBSD band contrast due to a higher degree of crystallinity (Fig. 3).

Grain 53 has many of the same features as Grain X. It comprises a CL type 1 core with low CL-response, and high U and Th concentrations that transition into a broad CL type 2 domain with lower U and Th, centred on a high CL response front (Fig. 3; Supplementary Fig. S-4). An ion imaging apparent date profile through the rim into the core reveals a CL type 3 edge domain (step 0–14 μm) with concordant to normally-discordant apparent $^{207}Pb^*/^{206}Pb^*$ dates as old as 3895 Ma, decreasing towards *ca.* 1800 Ma at the extreme edge of the profile (Fig. 4). Moving inwards through the crystal, a CL type 2 zone with highly-variable apparent dates corresponds to the high CL response front (step 14–33 μm). At a distinct low-U front, apparent $^{207}Pb^*/^{206}Pb^*$ ratios generally decrease and apparent $^{238}U/^{206}Pb^*$ ratios increase to produce extreme reverse discordance, implying U loss uncoupled to the degree of Pb mobility. Apparent $^{207}Pb^*/^{206}Pb^*$ dates within this reversely discordant front increase from ~3000 Ma at the rim ward edge to ~4000 Ma at the core side of the front. In the core, zircon with homogenous CL type 1a textures, higher U content, and low crystallinity has broadly concordant and less-variable $^{207}Pb^*/^{206}Pb^*$ dates (step 33–46 μm) of around 4000 Ma. The mottled CL type 1b area of the core of the grain is dominated by normal discordance with apparent $^{207}Pb^*/^{206}Pb^*$ dates as low as ~2400 Ma (Fig. 4).

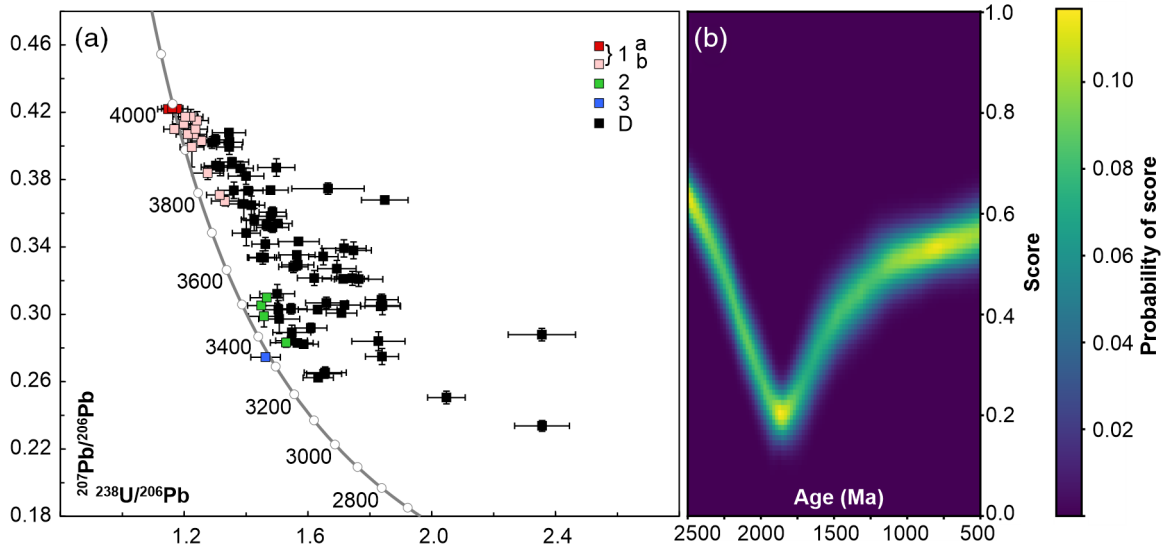

Figure 2 U–Pb geochronology of Acasta Gneiss zircon. **(a)** Inverse concordia. Colours denote interpreted CL groups. Red squares indicate Group 1a (resistive primary zircon core), pink squares indicate Group 1b (altered zircon core), green squares indicate Group 2 (analyses including younger zircon components), blue square indicates Group 3 (younger zircon overgrowth), black squares indicate Group D (>5 % discordant). Uncertainty shown at the two-sigma level. **(b)** Kolmogorov–Smirnov distance score between modelled upper intercept date for discordant *versus* concordant zircon population (within two sigma of concordia), calculated across all possible radiogenic-Pb loss times (see Kirkland *et al.*, 2020). The lowest distance score indicates greatest similarity in date structure and most likely time of Pb mobility. Colour scale is the probability estimate for KS score from bootstrapping.

Primary age Signature

An important question in the interpretation of the U–Pb geochronology of the studied zircon crystals from Acasta is the degree of secondary (post-magmatic) modification of primary isotopic ratios. Specifically, whether the various (near) concordant Eoarchean to Mesoarchean dates reflect new zircon growth or variable ancient radiogenic-Pb loss.

The oldest dates in this study comprise three concordant analyses of the homogeneous core domain (Group 1a) of Grain X, which yield a weighted mean date of 3990 ± 2 Ma. Under CL, this grain reveals a homogeneous rim with high-CL-response front (CL type 2) and a low-CL-response core (CL type 1). The core contains both homogeneous domains (CL type 1a) and mottled domains with reticulated alteration patterns (CL type 1b). The extremely low EBSD band-contrast response of this core suggests a low degree of crystallinity. Notwithstanding, homogeneous sites within the core preserve concordant U–Pb systematics (CL type 1a).

The concordant core analyses have high U (>891 ppm) and Th (>737 ppm) contents and, based on alpha dose calculations (Murakami *et al.*, 1991), are predicted to be in a highly metamict state (with 23.6–28.6 x 10^{15} alpha events assuming no post-crystallisation annealing). However, at 3520–3380 Ma, the best estimate for the time of their recrystallisation some 500 Ma after their magmatic growth (CL type 2; Fig. 2), calculations indicate that this core would have still been crystalline (1.8 x 10^{15} alpha events). Despite the extreme accumulated radiation damage implied by the EBSD data, the core of Grain X has concordant U–Pb systematics. We interpret the apparent lack of radiogenic-Pb loss in this core to indicate that it did not interact with secondary fluids, either at the time of recrystallisation or later. These observations are consistent with the concept that diffusive transport of U and Pb in zircon requires both a diffusion network and the presence of fluids (Pidgeon *et al.*, 1966; Geisler *et al.*, 2002; Herrmann *et al.*, 2021). Importantly, in isolation, radiation damage seems not to affect mobility of U or Pb.

In contrast to the concordant CL type 1a core domains that preserve Eoarchean dates, CL type 1b core domains are characterised by a mottled CL response; EBSD analysis reveals variable and highly-convoluted patterns (Fig. 3). The ion image for Grain 53 reveals a small CL type 1a core domain with consistent U/Pb* and Pb*/Pb* dates of *ca*. 4.0 Ga. This domain is in textural continuity with reticulated CL type 1b core domains that show high- to very-high normal discordance and are interpreted to have lost radiogenic Pb. Thus, small type 1a areas, as in the core of Grain X, appear to represent relict metamict core regions that remained isolated from fluids, and which consequently preserve concordant earliest Eoarchean dates.

Based on our data, the 3990 ± 2 Ma date for the three CL type 1a analyses is interpreted as the minimum crystallisation age of the magmatic protolith to the gneiss, consistent with the general distribution of data away from this point on the concordia diagram (Fig. 2). Given the evidence for multiple episodes of radiogenic-Pb mobility, the time at which radiogenic Pb loss occurred may be estimated using a Concordance–Discordance–Comparison test (Kirkland *et al.*, 2020). Application of this test indicates that the greatest similarity between the discordant and the concordant populations is achieved for a radiogenic Pb loss event at 1854 +101/–81 Ma (Fig. 2b). This age, which matches the youngest outermost concordant component of the CL type 3 domain on the ion image profile from Grain 53 (Fig. 4), is contemporaneous with the Paleoproterozoic Wopmay Orogeny that affected the western part of the Slave Province as part of the assembly of the Columbia supercontinent (Fisher *et al.*, 2020). Apatite (re) growth in the AGC has also been ascribed to this event (Antoine *et al.*, 2020; Fisher *et al.*, 2020). We interpret the U–Pb systematics to reflect a ≥3990 ± 2 Ma magmatic rock that underwent episodes of Pb mobility at 3965 Ma, 3520–3380 Ma, and *ca*. 1850 Ma within those portions of grains that had access to fluids (Iizuka *et al.*, 2007; Guitreau *et al.*, 2018; Kirkland *et al.*, 2020).

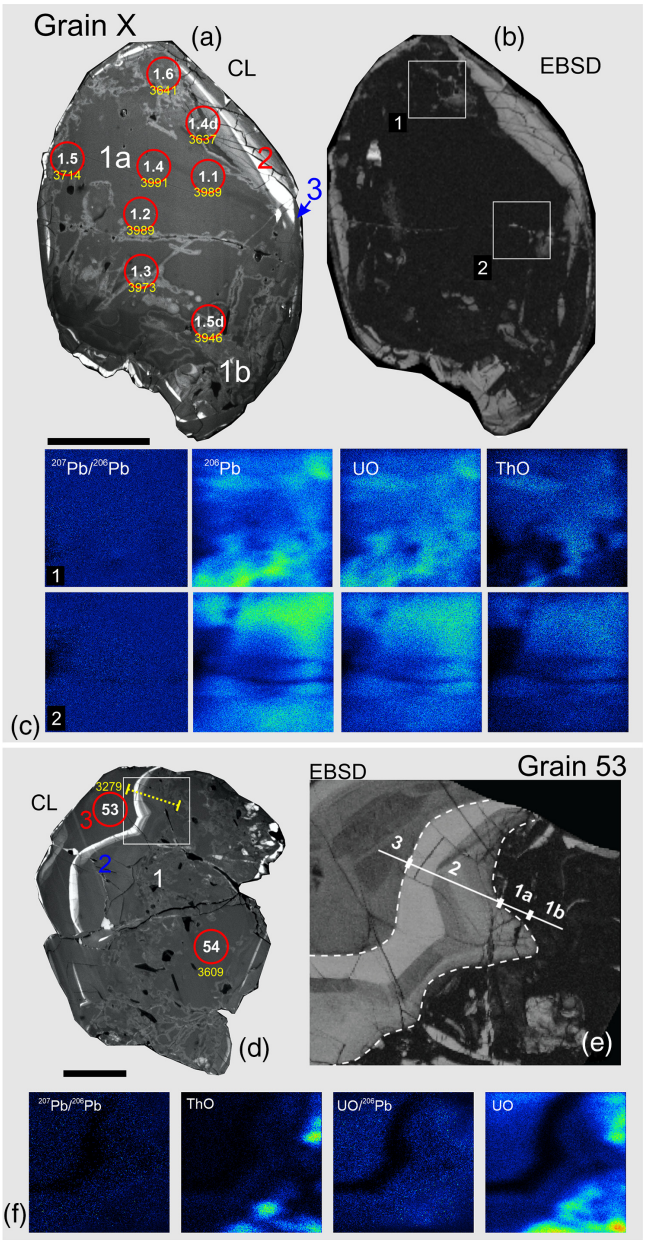

Figure 3 Images of Acasta Gneiss zircon. **(a and d)** Cathodoluminescence (CL). **(b and e)** Electron Backscatter Diffraction (EBSD) band contrast. **(c and f)** Ion images for the indicated isotopic masses and ratios. Brighter colours denote higher counts. Coloured text (1, 2, and 3) on the CL image denotes different CL types. U–Pb zircon analytical spots are shown as red circles (with $^{207}Pb^*/^{206}Pb^*$ dates in yellow font). Scale bars are 50 μm. Yellow dashed line in d is the apparent date transect shown in Fig. 4.

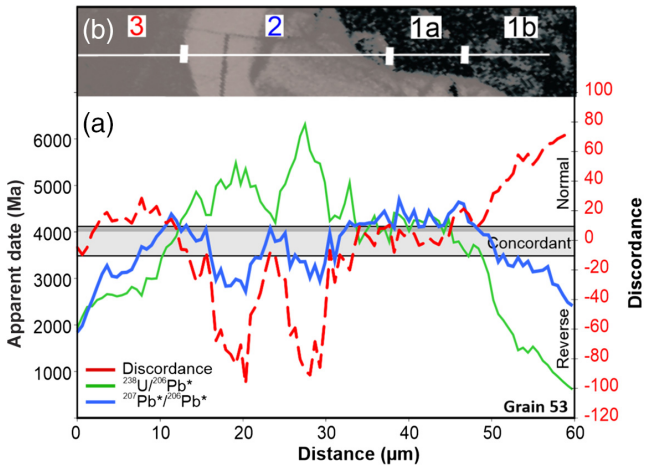

Figure 4 **(a)** Plot of apparent dates from ion image traverse. Dates calculated by moving a box (5 μm by 5 μm) along transect line shown in figure 3d. Primary age of Acasta indicated by thin dark grey box. Light grey box depicts +10 to –10 % U–Pb concordance. **(b)** Band contrast image of the zircon traverse line.

Recrystallisation

Ion imaging reveals a spatial variation in apparent dates within the crystalline domain (CL type 2) surrounding the core (CL type 1) in Grain 53 (Fig. 3). This region contains significant variation in composition along the axis of the recrystallisation front, with deviations to reverse discordance coupled with low-U concentrations, compatible with the loss of U to a fluid. This apparent date pattern is consistent with the low-U front representing a zone of recrystallisation, with U flushed out to the grain margin (Nasdala *et al.*, 2010; Putnis and Austrheim, 2013). The region behind (rim-ward of) the recrystallisation front (CL type 3) shows less reverse discordance. This rim region may comprise several different growth domains, with one likely age component estimated by a concordant 3332 ± 12 Ma analysis (CL type 3), requiring either expulsion of all earlier-formed radiogenic Pb or new zircon growth. Thus, we interpret the apparent date cross section to image a frozen alteration front transiting through the grain from rim to core, leaving a homogenised rind (Geisler *et al.*, 2007) onto which later zircon precipitated (*e.g.*, CL type 3).

Figure 4 implies at least two distinct alteration processes: radiogenic Pb loss from metamict cores leading to normal U–Pb discordance, and U dissociation from Pb leaving a reversely discordant front. Generally, Pb is considered to be more mobile than U in zircon (Pidgeon *et al.*, 1966). However, hydrothermal experiments on zircon have demonstrated enhanced U mobility in saline solutions (Geisler *et al.*, 2003). The front shows no noticeable reduction in Zr, but a slight decrease in Hf (Supplementary Fig. S-4), supporting a dissolution–recrystallisation mechanism producing zircon with reduced trace element concentrations (Geisler *et al.*, 2007). Importantly, as this new zircon is reversely discordant, it incorporated some unsupported Pb directly from the core, decoupling parent U from radiogenic Pb (Mattinson *et al.*, 1995). This implies that metamict cores interacted with fluids, losing volume and mass to a metamorphic liquid that facilitated recrystallisation localised on the ancient grain margin.

This process has implications for U–Pb geochronology as, despite the lower U fronts in zircon being less susceptible to radiation damage, they are nonetheless discordant due to incorporation of disassociated radiogenic-Pb. Any analytical mixture with such a front and normally discordant core, dependent on the percentage of mixture, could result in an apparently concordant analysis, yet having no age significance. Importantly, ion imaging provides a way to understand the process of alteration within geochronometers, ultimately helping to isolate domains in metamict zircon that still retain primary isotopic significance.

Acknowledgements

We thank the University of Oxford for the provision of material from the Moorbath Collection. S. Nemchin, J. Reimink, J. Kaempf, and C. Clark are thanked for comments that improved

the presentation of our arguments. M. Aleshin is thanked for SIMS technical support. J. Snape and R. Tartèse are thanked for their constructive reviews.

Editor: Romain Tartèse

Additional Information

Supplementary Information accompanies this letter at https://www.geochemicalperspectivesletters.org/article2332.

Cite this letter as: Kirkland, C.L., Johnson, T.E., Gillespie, J., Martin, L. (2023) Ion imaging of ancient zircon. *Geochem. Persp. Let.* 27, 38–42. https://doi.org/10.7185/geochemlet.2332

References

Antoine, C., Bruand, E., Guitreau, M., Devidal, J.L. (2020) Understanding Preservation of Primary Signatures in Apatite by Comparing Matrix and Zircon-Hosted Crystals From the Eoarchean Acasta Gneiss Complex (Canada). *Geochemistry, Geophysics, Geosystems* 21, e2020GC008923. https://doi.org/10.1029/2020GC008923

Bowring, S.A., Williams, I.S. (1999) Priscoan (4.00-4.03 Ga) orthogneisses from northwestern Canada. *Contributions to Mineralogy and Petrology* 134, 3–16. https://doi.org/10.1007/s004100050465

Fisher, C.M., Bauer, A.M., Vervoort, J.D. (2020) Disturbances in the Sm–Nd isotope system of the Acasta Gneiss Complex—Implications for the Nd isotope record of the early Earth. *Earth and Planetary Science Letters* 530, 115900. https://doi.org/10.1016/j.epsl.2019.115900

Ge, R., Wilde, S.A., Nemchin, A.A., Whitehouse, M.J., Bellucci, J.J., Erickson, T.M., Frew, A., Thern, E.R. (2018) A 4463 Ma apparent zircon age from the Jack Hills (Western Australia) resulting from ancient Pb mobilization. *Geology* 46, 303–306. https://doi.org/10.1130/G39894.1

Ge, R., Wilde, S.A., Nemchin, A.A., Whitehouse, M.J., Bellucci, J.J., Erickson, T.M. (2019) Mechanisms and consequences of intra-crystalline enrichment of ancient radiogenic Pb in detrital Hadean zircons from the Jack Hills, Western Australia. *Earth and Planetary Science Letters* 517, 38–49. https://doi.org/10.1016/j.epsl.2019.04.005

Geisler, T., Pidgeon, R.T., Van Bronswijk, W., Kurtz, R. (2002) Transport of uranium, thorium, and lead in metamict zircon under low-temperature hydrothermal conditions. *Chemical Geology* 191, 141–154. https://doi.org/10.1016/S0009-2541(02)00153-5

Geisler, T., Pidgeon, R.T., Kurtz, R., van Bronswijk, W., Schleicher, H. (2003) Experimental hydrothermal alteration of partially metamict zircon. *American Mineralogist* 88, 1496–1513. https://doi.org/10.2138/am-2003-1013

Geisler, T., Schaltegger, U., Tomaschek, F. (2007) Re-equilibration of zircon in aqueous fluids and melts. *Elements* 3, 43–50. https://doi.org/10.2113/gselements.3.1.43

Guitreau, M., Mora, N., Paquette, J.L. (2018) Crystallization and Disturbance Histories of Single Zircon Crystals From Hadean-Eoarchean Acasta Gneisses Examined by LA-ICP-MS U-Pb Traverses. *Geochemistry, Geophysics, Geosystems* 19, 272–291. https://doi.org/10.1002/2017GC007310

Harley, S.L., Kelly, N.M. (2007) Zircon Tiny but Timely. *Elements* 3, 13–18. https://doi.org/10.2113/gselements.3.1.13

Harley, S.L., Kelly, N.M., Möller, A. (2007) Zircon behaviour and the thermal histories of moutain chains. *Elements* 3, 25–30. https://doi.org/10.2113/gselements.3.1.25

Herrmann, M., Söderlund, U., Scherstén, A., Næraa, T., Holm-Alwmark, S., Alwmark, C. (2021) The effect of low-temperature annealing on discordance of U–Pb zircon ages. *Scientific Reports* 11, 7079. https://doi.org/10.1038/s41598-021-86449-y

Iizuka, T., Komiya, T., Ueno, Y., Katayama, I., Uehara, Y., Maruyama, S., Hirata, T., Johnson, S.P., Dunkley, D.J. (2007) Geology and zircon geochronology of the Acasta Gneiss Complex, northwestern Canada: New constraints on its tectonothermal history. *Precambrian Research* 153, 179–208. https://doi.org/10.1016/j.precamres.2006.11.017

Kirkland, C.L., Johnson, T.E., Kinny, P.D., Kapitany, T. (2020) Modelling U-Pb discordance in the Acasta Gneiss: Implications for fluid–rock interaction in Earth's oldest dated crust. *Gondwana Research* 77, 223–237. https://doi.org/10.1016/j.gr.2019.07.017

Kusiak, M.A., Whitehouse, M.J., Wilde, S.A., Nemchin, A.A., Clark, C. (2013) Mobilization of radiogenic Pb in zircon revealed by ion imaging: Implications for early Earth geochronology. *Geology* 41, 291–294. https://doi.org/10.1130/G33920.1

Mattinson, J.M., Graubard, C.M., Parkinson, D.L., McClelland, W.C. (1995) U-Pb reverse discordance in zircons: The role of fine-scale oscillatory zoning and sub-micron transport of Pb. *Geophysical Monograph Series* 95, 355–370. https://doi.org/10.1029/GM095p0355

Moorbath, S., Whitehouse, M.J., Kamber, B.S. (1997) Extreme Nd-isotope heterogeneity in the early Archaean - Fact or fiction? Case histories from northern Canada and West Greenland. *Chemical Geology* 135, 213–231. https://doi.org/10.1016/S0009-2541(96)00117-9

Murakami, T., Chakoumakos, B.C., Ewing, R.C., Lumpkin, G.R., Weber, W.J. (1991) Alpha-decay event damage in zircon. *American Mineralogist* 76, 1510–1532.

Nasdala, L. (1998) Metamictization and U-Pb isotopic discordance in single zircons: A combined Raman microprobe and SHRIMP ion probe study. *Mineralogy and Petrology* 62, 1–27. https://doi.org/10.1007/BF01173760

Nasdala, L., Hanchar, J.M., Rhede, D., Kennedy, A.K., Váczi, T. (2010) Retention of uranium in complexly altered zircon: An example from Bancroft, Ontario. *Chemical Geology* 269, 290–300. https://doi.org/10.1016/j.chemgeo.2009.10.004

Pidgeon, R.T., O'Neil, J.R., Silver, L.T. (1966) Uranium and Lead Isotopic Stability in a Metamict Zircon under Experimental Hydrothermal Conditions. *Science* 154, 1538–1540. https://doi.org/10.1126/science.154.3756.1538

Pidgeon, R.T., Nemchin, A.A., Whitehouse, M.J. (2017) The effect of weathering on U-Th-Pb and oxygen isotope systems of ancient zircons from the Jack Hills, Western Australia. *Geochimica et Cosmochimica Acta* 197, 142–166. https://doi.org/10.1016/j.gca.2016.10.005

Putnis, A., Austrheim, H. (2013) Mechanisms of metasomatism and metamorphism on the local mineral scale: The role of dissolution-reprecipitation during mineral re-equilibration. In: D.E. Harlov, and H. Austrheim, (Eds.) *Metasomatism and the chemical transformation of rock: the role of fluids in terrestrial and extraterrestrial processes*. Lecture Notes in Earth System Sciences, Germany, Springer, 141–170. https://doi.org/10.1007/978-3-642-28394-9_5

Reimink, J.R., Chacko, T., Stern, R.A., Heaman, L.M. (2014) Earth's earliest evolved crust generated in an Iceland-like setting. *Nature Geoscience* 7, 529–533. https://doi.org/10.1038/ngeo2170

Reimink, J.R., Chacko, T., Stern, R.A., Heaman, L.M. (2016) The birth of a cratonic nucleus: Lithogeochemical evolution of the 4.02-2.94 Ga Acasta Gneiss Complex. *Precambrian Research* 281, 453–472. https://doi.org/10.1016/j.precamres.2016.06.007

Stern, R.A., Bleeker, W. (1998) Age of the world's oldest rocks refined using Canada's SHRIMP: the Acasta Gneiss Complex, Northwest Territories, Canada. *Geoscience Canada* 25, 27–31.

Trail, D., Cherniak, D.J., Watson, E.B., Harrison, T.M., Weiss, B.P., Szumila, I. (2016) Li zoning in zircon as a potential geospeedometer and peak temperature indicator. *Contributions to Mineralogy and Petrology* 171, 25. https://doi.org/10.1007/s00410-016-1238-8

Valley, J.W., Reinhard, D.A., Cavosie, A.J., Ushikubo, T., Lawrence, D.F., Larson, D.J., Kelly, T.F., Snoeyenbos, D.R., Strickland, A. (2015) Presidential Address. Nano- and micro-geochronology in Hadean and Archean zircons by atom-probe tomography and SIMS: New tools for old minerals. *American Mineralogist* 100, 1355–1377. https://doi.org/10.2138/am-2015-5134

Ward, P.D., Brownlee, D. (2000). *Rare Earth: Why Complex Life is Uncommon in the Universe*. Copernicus, New York. ISBN: 978-0-387-95289-5. https://doi.org/10.1007/b97646

Willbold, M., Mojzsis, S.J., Chen, H.W., Elliott, T. (2015) Tungsten isotope composition of the Acasta Gneiss Complex. *Earth and Planetary Science Letters* 419, 168–177. https://doi.org/10.1016/j.epsl.2015.02.040

Geochemical Perspectives Letters

Ion imaging of ancient zircon

C.L. Kirkland, T.E. Johnson, J. Gillespie, L. Martin

Supplementary Information

The Supplementary Information includes:

- Analytical Methods
- Tables S-1 and S-2
- Figures S-1 to S-4
- Supplementary Information References

Analytical methods

SIMS U–Pb

Sample AC13 was collected by Stephen Moorbath from the University of Oxford in July 1995, from 500 metres NNW of the Acasta camp. Zircon crystals from sample AC13 were analysed for U–Th–Pb isotopes using the SHRIMP II ion probe at Curtin University following standard operating procedures (Wingate and Kirkland, 2014). The zircon surface was sputtered with a primary, mass-filtered $(O_2)^-$ beam with ~ 2 nA current, focused to a ~ 15 μm spot. The mass resolution, M/ΔM, was better than 5000. Twenty-two analyses of the 91500 zircon reference material (Wiedenbeck *et al.*, 1995) were obtained during the session, all of which indicate an external spot-to-spot (reproducibility) uncertainty of 1.33% (1σ) and a $^{238}U/^{206}Pb^*$ calibration uncertainty of 0.45% (1σ). These calibration uncertainties are included in the calculated uncertainties on $^{238}U/^{206}Pb^*$ ratios and dates listed in Table S1. The OG1 zircon reference material was analysed as an unknown and yielded a weighted mean $^{207}Pb^*/^{206}Pb^*$ age of 3458 ± 7 Ma (MSWD = 0.51, n = 5), within accepted values (Stern *et al.*, 2009). No fractionation correction on $^{207}Pb/^{206}Pb$ was deemed necessary. Common-Pb corrections were applied to all analyses using contemporaneous common Pb determined according to the model of Stacey and Kramers (1975) based on ^{204}Pb counts. The Excel-based program Squid 2 (Ludwig, 2001) was used for data processing and data were plotted using Isoplot (Ludwig, 2003).

SIMS ion imaging

Ion imaging to map the U and Pb isotopic composition of zircon was performed with a Cameca 1280 ion microprobe equipped with a high-brightness Oregon Physics Hyperion-II RF-plasma oxygen ion source at the University of Western Australia. Prior to analysis, the sample mount was cleaned with ethanol, dried, and a ~10 nm gold coating applied. A mass filtered $^{16}O^-$ 500 pA primary ion beam was focussed in Gaussian mode and rastered over a 50 x 50 μm area. A larger 65 x 65 μm area was pre-sputtered for 15 minutes to remove gold coating and limit the effects of surface contamination. This procedure was followed by automatic centring of the secondary ion beam in the 3000 μm field aperture and optimisation of mass calibration, performed

automatically for each run using the $^{90}Zr_2{}^{16}O+$ species at a nominal mass of 196. During analysis, the sample chamber was flooded with oxygen to enhance Pb ion yields (Schuhmacher *et al*., 1994). The secondary ions of $^{177}Hf^{16}O$, $^{90}Zr_2{}^{16}O$, ^{204}Pb, ^{206}Pb, ^{207}Pb, ^{208}Pb, background, ^{238}U, $^{232}Th^{16}O$, $^{238}U^{16}O$ and $^{238}U^{16}O_2$ were measured utilising a mass-skipping routine. All masses were measured on the H2 detector operating at a mass resolving power of ~4800, except for $^{177}Hf^{16}O$ and $^{90}Zr_2{}^{16}O$ that were measured on the L1 and H2 detectors, respectively, and Pb isotopes that were measured on L1 (^{204}Pb), C (^{206}Pb), H1 (^{207}Pb) and H2 (^{208}Pb). Images (resolution 512 x 512) were integrated over 100 planes, resulting in a total measurement time of 1 hour 14 minutes per image. The Cameca WinImage2 software was used to process the images (in plane accumulation mode) and to extract U–Pb ratios along profiles of interest via a 5 by 5 µm area moving along the profile line. Profile lines were normalised to counts along a line in the same orientation on the 91500 reference zircon (Wiedenbeck *et al*., 1995). Common Pb correction was applied to all ratios using measured ^{204}Pb counts and the terrestrial Pb evolution model of Stacy and Kramers (1975). Apparent dates across transects are given in Table S2.

Electron backscatter diffraction microstructural and cathodoluminescence imaging

CL imaging and EBSD mapping was conducted using a Tescan Mira3 field emission scanning electron microscope with an Oxford Instruments AZtec/Nordlys EBSD+EDX acquisition system in the John de Laeter Centre, Curtin University. Panchromatic CL images were collected on untilted samples using 10 kV acceleration voltage, whereas EBSD data were collected at a 70° tilt, 20 kV acceleration voltage, and 1.5 nA beam current. EBSD data were processed and visualised using AZtecCrystal, including a 'wildspike' correction to remove isolated erroneous pixels. Individual zircon grains were mapped using the match unit cell parameters of Hazen and Finger, (1979).

Supplementary Tables

Table S-1 Supplementary U–Pb data table (.xlsx)
Table S-2 Supplementary ion imaging traverse data table (.xlsx)

Table S-1 and S-2 (.xlsx) are available for download from the online version of this article at https://doi.org/10.7185/geochemlet.2332

Supplementary Figures

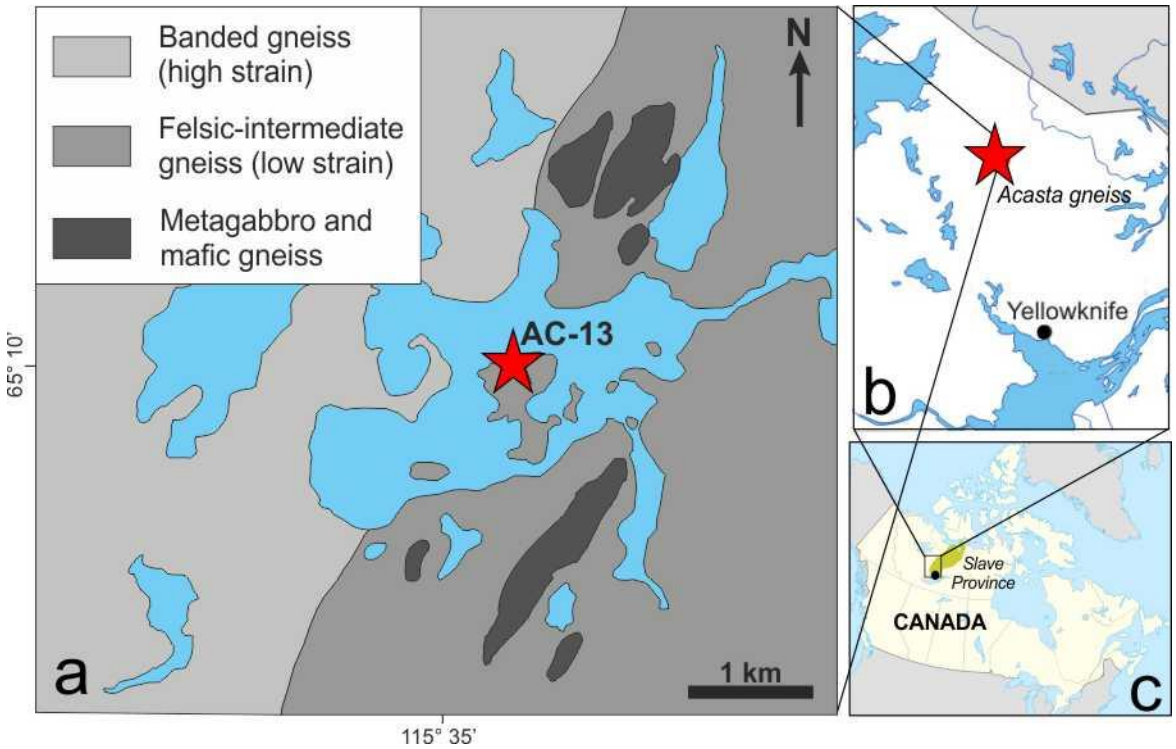

Figure S-1 Maps of the Acasta Gniess Complex region and wider surrounds. **(a)** Sketch map of the Acasta Gneiss Complex. The red star marks the location of the investigated sample. **(b)** Regional map of the Northwestern territories, Canada, with the AGC shown as a red star. **(c)** Map of Canada showing the location of the Slave Province.

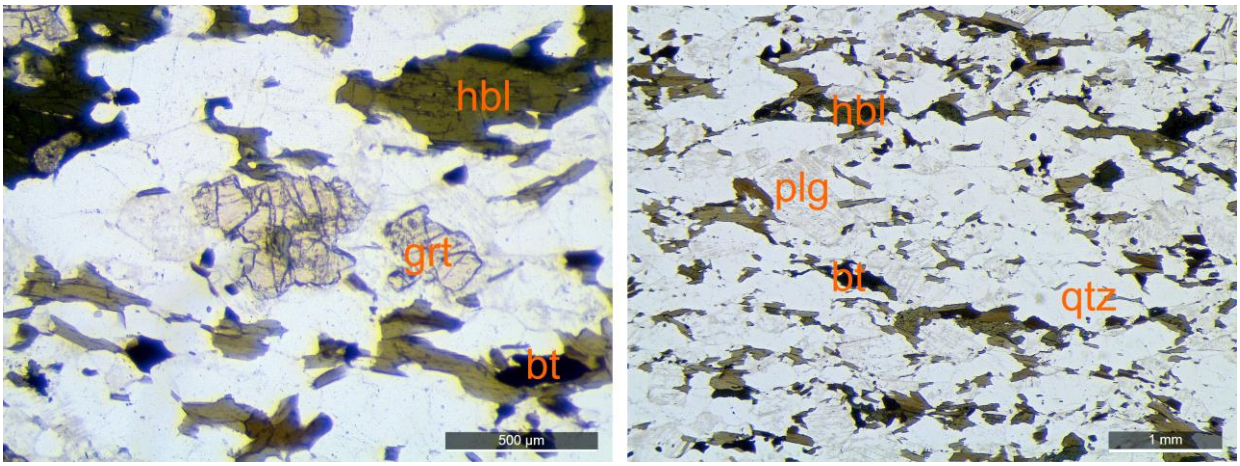

Figure S-2 Transmitted light photomicrographs of sample AC13 Idiwhaa gneiss, Acasta Gneiss Complex. Quartz (qtz), plagioclase (plg), biotite (bt), hornblende (hbl), and garnet (grt). Scale bars shown.

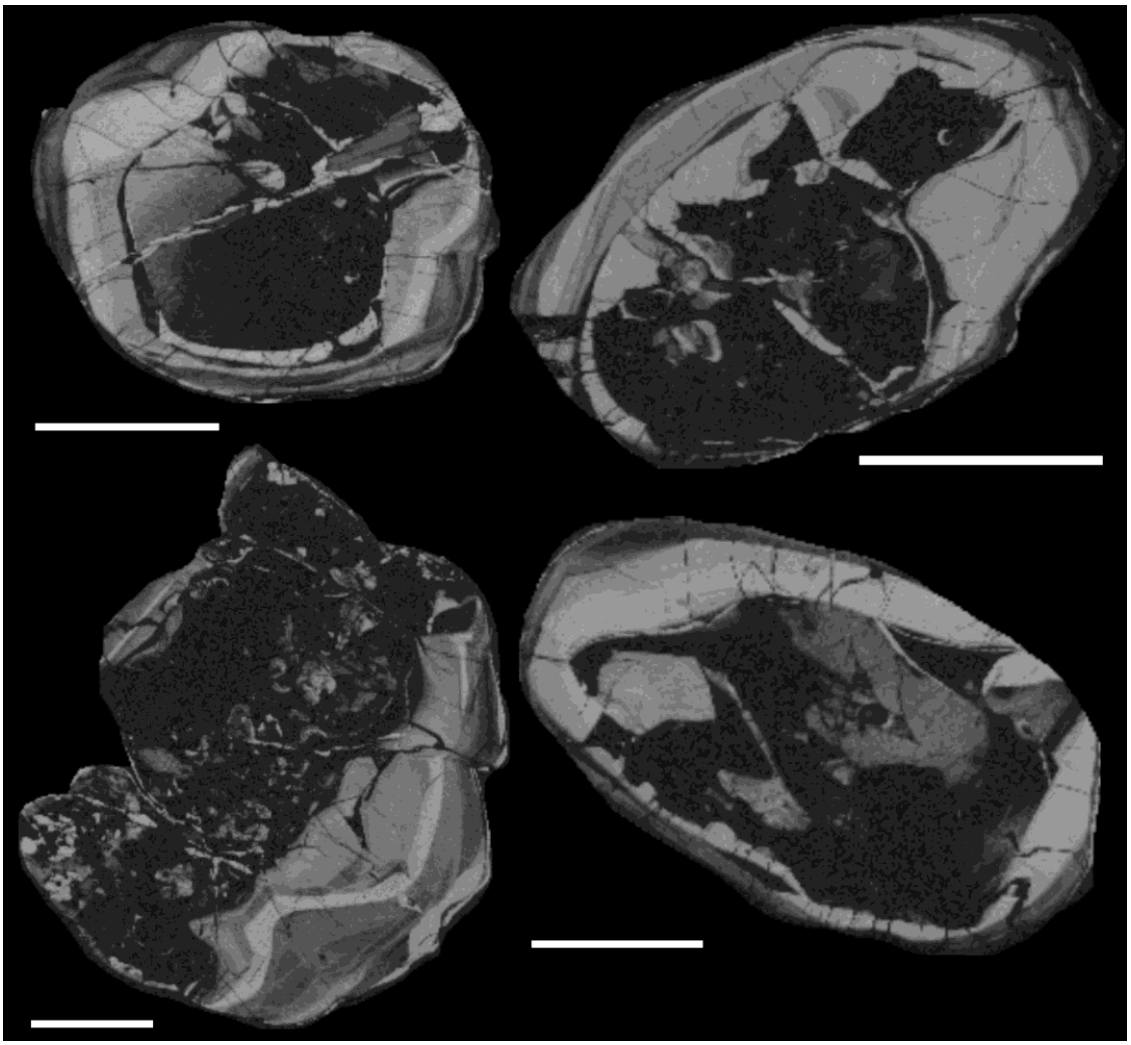

Figure S-3 Electron Backscatter Diffraction (EBSD) images of zircon grains. Representative EBSD band contrast images from zircon grains extracted from sample AC13, Idiwhaa gneiss, Acasta Gneiss Complex. Scale bar for each image is 50 μm.

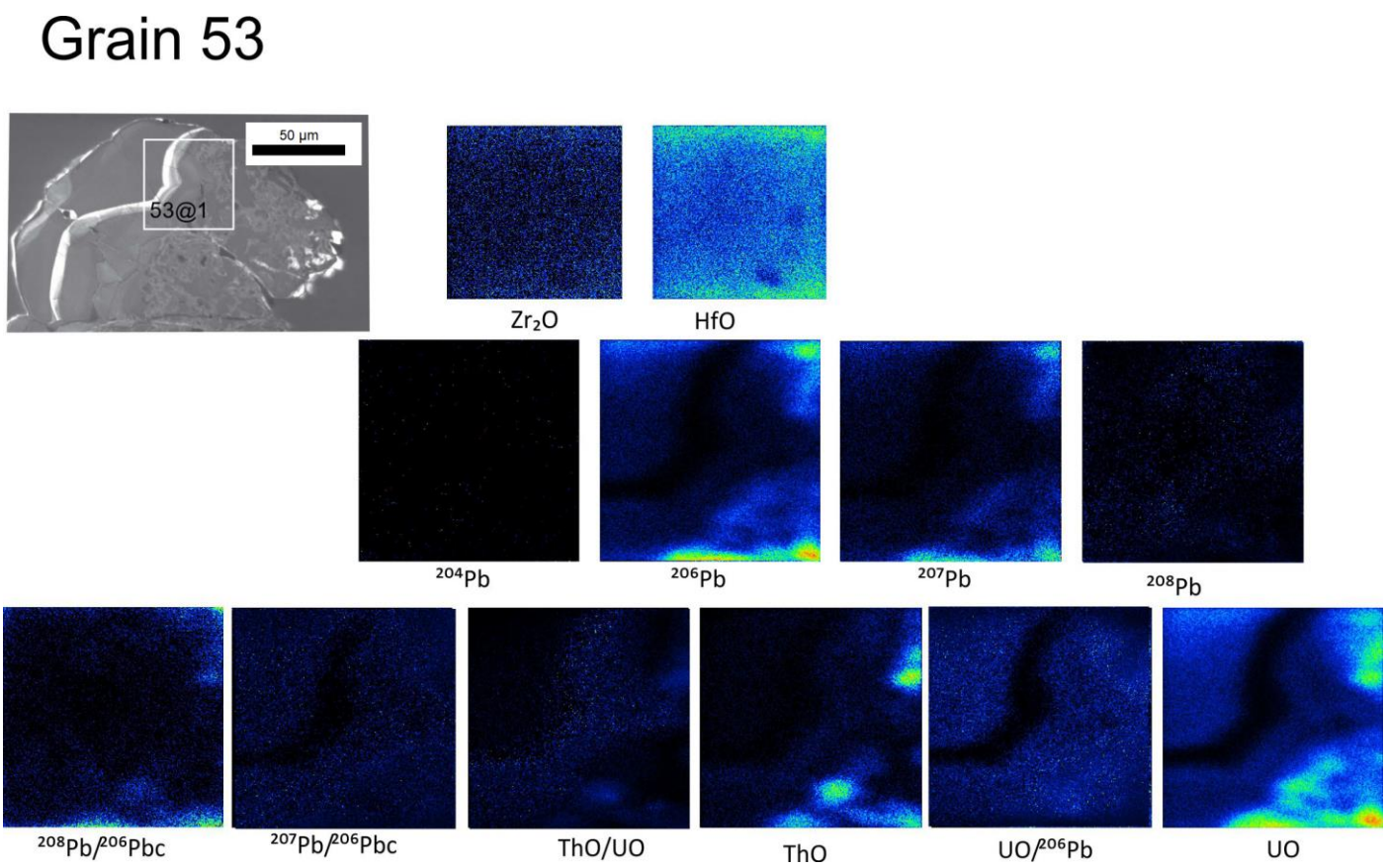

Figure S-4 Ion images of zircon Grain 53. Intensity of colour reflects cps for the indicated ratio, oxide, or isotope. Inset on the top left shows the location of the ion images on a reference cathodoluminescence image of the grain. A scale bar is provided in the cathodoluminescence image. All ion images are 50 x 50 µm.

Supplementary Information References

Hazen, R.M., Finger, L.W. (1979) Crystal structure and compressibility of zircon at high pressure. *American Mineralogist* 64, 196-201.

Ludwig, K. (2001) Squid 1.02: A user's manual. Berkeley Geochronology Center Special Publication, 2, 19pp.

Ludwig, K.R. (2003) User's manual for isoplot 3.00, a geochronological toolkit for microsoft excel. Berkeley Geochronl. Cent. Spec. Publ., 4, 25-32.

Schuhmacher, M., Chambost, E.D., McKeegan, K.D., Harrison, T.M., Migeon, H. (1994) In situ dating of zircon with the Cameca IMS 1270. In: A. Benninghoven, B. Hagenhoff, and H.W. Werner (Eds.), *Secondary Ion Mass Spectrometry SIMS IX*, Chichester, U.K., John Wiley, 919 – 922.

Stacey, J.S., Kramers, J.D. (1975) Approximation of terrestrial lead isotope evolution by a two-stage model. *Earth and Planetary Science Letters*, 26, 207-221. https://doi.org/10.1016/0012-821X(75)90088-6

Stern, R.A., Bodorkos, S., Kamo, S.L., Hickman, A.H., Corfu, F.Y. (2009) Measurement of SIMS instrumental mass fractionation of Pb isotopes during zircon dating. *Geostandards and Geoanalytical Research*, 33, 145-168. https://doi.org/10.1111/j.1751-908X.2009.00023.x

Wiedenbeck, M., Alle, P., Corfu, F.Y., Griffin, W.L., Meier, M., Oberli, F., Quadt, A.V., Roddick, J.C., Spiegel, W. (1995) Three natural zircon standards for U-Th-Pb, Lu-Hf, trace element and REE analysis. *Geostandards Newsletter*, 19, 1-23. https://doi.org/10.1111/j.1751-908X.1995.tb00147.x

Wingate, M.T.D., Kirkland, C.L. (2014) Introduction to Geochronology Information Released in 2014. East Perth, *Geological Survey of Western Australia*, http://www.dmp.wa.gov.au/geochron